

**FULL ARTICLE**

# *In vivo* study of metabolic dynamics and heterogeneity in brown and beige fat by label-free multiphoton redox and fluorescence lifetime microscopy

Sicong He<sup>1,2,3</sup>  | Xiuqing Wei<sup>2,3,4</sup> | Zhongya Qin<sup>1,2,3</sup> | Congping Chen<sup>1,2,3</sup> |  
 Zhenguo Wu<sup>2,3,4\*</sup> | Jianan Y. Qu<sup>1,2,3\*</sup>

<sup>1</sup>Department of Electronic and Computer Engineering, Hong Kong University of Science and Technology, Kowloon, Hong Kong, People's Republic of China

<sup>2</sup>State Key Laboratory of Molecular Neuroscience, Hong Kong University of Science and Technology, Kowloon, Hong Kong, People's Republic of China

<sup>3</sup>Center of Systems Biology and Human Health, Hong Kong University of Science and Technology, Kowloon, Hong Kong, People's Republic of China

<sup>4</sup>Division of Life Science, Center for Stem Cell Research, Hong Kong University of Science and Technology, Kowloon, Hong Kong, People's Republic of China

**\*Correspondence**

Prof. Zhenguo Wu, State Key Laboratory of Molecular Neuroscience, Center for Stem Cell Research, Center of Systems Biology and Human Health, the Hong Kong University of Science and Technology, Clear Water Bay, Kowloon, Hong Kong, People's Republic of China.  
 Email: bczgwu@ust.hk

Prof. Jianan Y. Qu, Department of Electronic and Computer Engineering, Center of Systems Biology and Human Health, the Hong Kong University of Science and Technology, Clear Water Bay, Kowloon, Hong Kong, People's Republic of China.

Email: eequ@ust.hk

**Funding information**

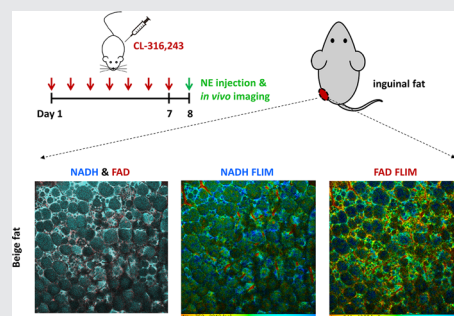
Hong Kong University of Science and Technology, Grant/Award Number: RPC10EG33; Research Grants Council, University Grants Committee, Grant/Award Numbers: 16102518, 16103215, 16148816, 662513, AOE/M-09/12, C6002-17GF, T13-605/18W, T13-607/12R, T13-706/11-1

**Abstract**

In this work, the metabolic characteristics of adipose tissues in live mouse model were investigated using a multiphoton redox ratio and fluorescence lifetime imaging technology. By analyzing the intrinsic fluorescence of metabolic coenzymes, we measured the optical redox ratios of adipocytes *in vivo* and studied their responses to thermogenesis. The fluorescence lifetime imaging further revealed changes in protein bindings of metabolic coenzymes in the adipocytes during thermogenesis. Our study uncovered significant heterogeneity in the cellular structures and metabolic characteristics of thermogenic adipocytes in brown and beige fat. Subgroups of brown and beige adipocytes were identified based on the distinct lipid size distributions, redox ratios, fluorescence lifetimes and thermogenic capacities. The results of our study show that this label-free imaging technique can shed new light on *in vivo* study of metabolic dynamics and heterogeneity of adipose tissues in live organisms.

**KEYWORDS**

beige fat, fluorescence lifetime, optical redox ratio, thermogenesis



## 1 | INTRODUCTION

Brown adipose tissue (BAT) and white adipose tissue (WAT) are two main types of fat in mammals. BAT is a thermoregulatory organ that can dissipate energy as heat through nonshivering thermogenesis. It plays a fundamental role in regulating whole-body glucose homeostasis and insulin sensitivity [1]. In contrast, WAT exhibits opposing functions and is mainly responsible for storing excess energy. Recently, a new type of thermogenic adipocyte was uncovered in specific WAT depots, namely, beige/brite (brown-in-white) adipocyte [2–4]. Beige adipocytes can be generated in WAT by cold exposure or by other approaches, such as  $\beta$ 3-adrenergic receptor (ADRB3) agonists stimulation [5, 6]. Similar to BAT, beige fat is also competent for thermogenesis under the mediation of a specialized mitochondrial protein, uncoupled protein 1 (UCP1) [7, 8]. With the discovery of thermogenic adipocytes in adult humans, therapeutic interest has been focused on the stimulation of brown and/or beige fat biogenesis and enhancement of thermogenesis to combat obesity and insulin resistance [9, 10].

In vivo metabolic monitoring of brown and beige adipocytes in mouse model is of great significance for understanding the mechanisms underlying thermogenesis. However, the traditional metabolic measurement tools are not able to specifically assess the thermogenic characteristics of brown and beige fat. The Seahorse Extracellular Flux Analyzer is a prevalent approach to measuring the oxygen consumption rate (OCR) of isolated adipocytes [11, 12], and it has been reported that the OCR of brown adipocytes increases after the activation of thermogenesis by norepinephrine (NE) treatment [13]. The major limitation of Seahorse instrument is unable to measure the fat metabolism in live animal. Thermal imaging allows noninvasive measurement of the temperature change in BAT during thermogenesis. However, it is inaccurate for metabolic characterization of beige fat, because the heat locally produced in interscapular BAT can quickly redistribute throughout the animal body via blood circulation and raise the temperature of beige fat in the inguinal region [14]. Positron emission tomography and optoacoustic detection have been used for real-time measurement of BAT metabolic activity in mouse and human [15–17], but they cannot achieve cellular resolution, preventing rigorous study on metabolic heterogeneity in adipocytes [18]. Other measurements such as blood flow, food intake and locomotor activity [19–21] are all short of specificity and are incapable of distinguishing the metabolism of brown and beige fat from that of the entire organism.

The mitochondrial metabolic coenzymes, reduced nicotinamide adenine dinucleotide (NADH) and flavin

adenine dinucleotide (FAD), are two major endogenous fluorophores in cells and play crucial roles in metabolic and transcriptional regulation [22–24]. They are intensively involved in two critical biochemical processes in mitochondria (Figure S1). The first process is  $\beta$ -oxidation of fatty acid, in which fatty acid molecules are broken down to produce acetyl-CoA, while  $\text{NAD}^+$  and FAD are reduced to form NADH and  $\text{FADH}_2$ . In the second process, NADH and  $\text{FADH}_2$  are oxidized to generate  $\text{NAD}^+$  and FAD via the electron transport chain (ETC) [8, 25]. Therefore, the optical redox ratio (ORR) was defined as the relative fluorescence intensity of NADH and FAD, and the oxidation-reduction ratio in mitochondria can be evaluated by the ORR using label-free fluorescence microscopy. Over the past decades, the ORR has been widely used as an intrinsic indicator of redox states in cells and tissues [26–28]. In our recent work, the ORR was used to monitor the thermogenesis of BAT in vivo [14]. We found that the ORR of BAT increases significantly after NE injection in mice, which is correlated with the temperature rise in BAT induced by thermogenesis [14]. The result suggests that redox ratio imaging could probe the accelerated  $\beta$ -oxidation and enhanced metabolic activity in thermogenic adipocytes. This may provide opportunities to investigate the metabolic characteristics of beige fat at subcellular resolution in vivo, which has not been conducted in live animal model. In addition to redox ratio imaging, fluorescence lifetime imaging microscopy (FLIM) has also been used for mapping of cellular metabolism [29–31] and detection of pathogens [32]. NADH and FAD exhibit distinct fluorescence lifetimes (FLT) in free and protein-bound forms, and the free-to-bound ratios of NADH or FAD can be used to discriminate different cellular metabolic states [33–36]. It was recently documented that the brown and white fat exhibit distinctive FLT signatures [37]. Hence, FLIM may provide complementary insights into the unique metabolic characteristics of thermogenic adipocytes.

In this study, we simultaneously image subcellular morphology and quantify the cellular metabolism in adipose tissues in vivo. Using a multiphoton redox ratio and FLT imaging system, we study the significant changes in ORRs and free-to-bound ratios of NADH (FLT:  $335 \pm 18$  and  $2160 \pm 83$  ps in free and protein-bound forms, respectively) and FAD (FLT:  $209 \pm 21$  and  $1981 \pm 174$  ps in protein-bound and free forms, respectively) in brown and beige fat during NE-induced thermogenesis. In addition, the heterogeneity of cellular structures and metabolic states in brown and beige fat are investigated. Our findings provide clear evidences that adipocytes with unique lipid size distributions, ORRs and FLT exhibit distinct thermogenic competence. We

demonstrate that the ORR and FLT of mitochondrial coenzymes can be used as label-free biomarkers to study the thermogenesis of brown and beige fat.

## 2 | METHODS AND MATERIALS

### 2.1 | Animals

The C57BL/6J mouse model was used in this study. Mice were housed in a 12:12 light:dark cycle, and were randomized to respective groups without restrictions. To induce beige fat in the inguinal WAT, the mice were administered one dose of CL-316,243 (1 mg/Kg/day) for seven consecutive days through interperitoneal injection. For in vivo imaging experiments, mice were anesthetized by intraperitoneal injection of ketamine (0.133 mg/g of

body weight) in combination with xylazine (0.013 mg/g of body weight). Mouse skin around the interscapular and inguinal region was removed for BAT and WAT/beige fat imaging, respectively. The mice were given an intraperitoneal injection of NE (A7257, Sigma-Aldrich, 1  $\mu$ g/g of body weight) to activate thermogenesis. After the experiments, the mice were sacrificed by cervical dislocation. The study was approved by the Animal Ethics Committee of the Hong Kong University of Science and Technology.

### 2.2 | Multiphoton fluorescence microscope system with FLIM capability

The optical layout of the multiphoton fluorescence microscope system is shown in Figure 1A. A femtosecond

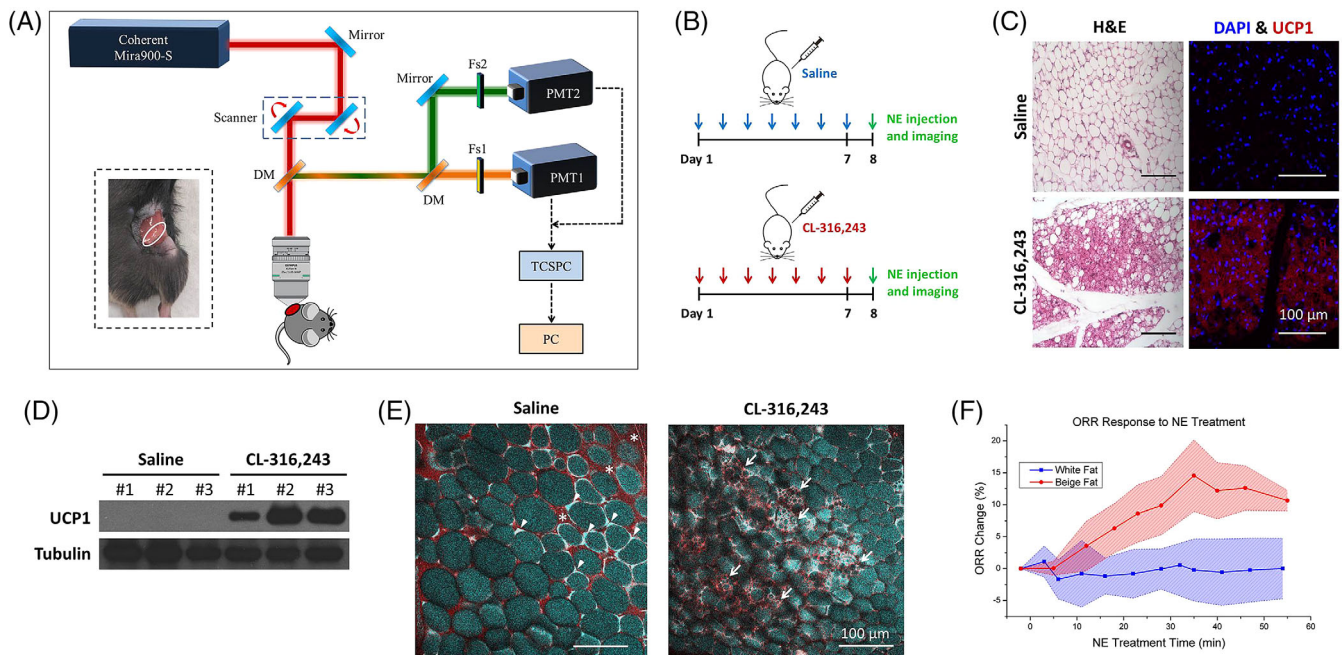


**FIGURE 1** In vivo ORR imaging of beige and white fat. A, Optical layout and block diagram of the multiphoton redox ratio and FLIM system. DM, dichroic mirror; Fs, filter set; PC, personal computer; PMT, photomultiplier tube; TCSPC, time-correlated single photon counting. The embedded figure shows the inguinal region of mouse for in vivo beige/white fat imaging. B, Schematic illustration of experiment design for in vivo fluorescence imaging of beige and white fat. One group of C57BL/6J mice was treated with the ADRB3 agonist CL-316,243 at 1 mg/kg for seven consecutive days to generate beige fat. The other group was treated with saline for 7 days. In vivo two-photon imaging was performed on the eighth day, and all the mice were injected with NE to activate thermogenesis. C, H&E staining and UCP1 immunostaining with Alexa Fluor 594 show that UCP1-abundant beige adipocytes containing small lipid droplets were found in the inguinal WAT of the mice treated with CL-316,243. Typical WAT phenotype was observed in the control group treated with saline. DAPI is used as a nuclear counterstain to visualize the adipocyte distributions. D, Western blotting results reveal the high UCP1 expression level in the inguinal fat of CL-316,243-treated mice. Tubulin was used as an internal control for protein loading. E, Pseudocolor TPEF images of the inguinal fat of mice treated with saline/CL-316,243. Fluorescence signals in NADH and FAD channels were coded in cyan and red, respectively. The saline-treated mice (left) contain white adipocytes with unilocular morphology only, while the CL-316,243-treated mice (right) show beige adipocytes embedded in the WAT. Arrowheads: the thin cytoplasm in white adipocytes. Asterisks: autofluorescence in the extracellular matrix of WAT detected in the FAD channel. Arrows: beige adipocytes containing multilocular lipids. F, Dynamic change in the cytoplasmic ORRs of beige and white fat during NE treatment in vivo. Each statistical curve is shown in terms of its average with its SD over the measurements from four mice

Ti:sapphire laser (Mira900-S, Coherent) with 140 fs pulse duration was tuned at 810 nm to excite the NADH and FAD fluorescence signals simultaneously [14, 38]. A water immersion objective (XLPLN25XWMP2, 1.05 NA, Olympus) was used to focus the excitation laser beam to the sample. The backward two-photon excited fluorescence (TPEF) signals were collected by the same laser-focusing objective and reflected to a fluorescence detection system by a dichroic mirror (FF665-Di02, Semrock). In the detection system, two hybrid detectors (HPM-100-40, Becker & Hickl) equipped with a time-correlated single photon counting (TCSPC) module (SPC-150, Becker & Hickl) were used to record time-resolved NADH (band-pass filter: FF02-447/60, Semrock) and FAD (band-pass filter: FF03-525/50, Semrock) signals simultaneously. A pair of galvanometer scanners was used to scan the laser beams to generate TPEF and FLIM images. The linearity of the hybrid detectors was validated by measuring the power-squared dependence of TPEF in the Rhodamine 6G solution (Figure S2) [39, 40]. In addition, the fluorescence anisotropy is insignificant in adipose tissues (Figure S3), so the fluorescence over all polarization orientations was collected for analysis [41]. The excitation laser power at the sample was 15 mW, and no apparent phototoxicity effect was observed (Figure S4).

### 2.3 | Analysis on ORR and FLT

First of all, the lipid droplets (LDs) in the adipocytes were validated with a stimulated Raman scattering (SRS) microscope [14], which enables label-free chemical imaging in adipose tissues (Figure S5). The SRS images and spectra suggest that the vacuoles structures in the fluorescence images of adipocytes were LDs enriched with triacylglycerol [14]. Before ORR and FLT analysis, image masks were generated by algorithms to extract the fluorescence signals in cytoplasm. Since the lipids and cytoplasm of adipocytes have distinct fluorescence spectra [14], the lipid fluorescence can be excluded using dual-channel ratiometric image masks (Figure S6). Additionally, the weak autofluorescence in the extracellular matrix of adipose tissues was also removed by setting an intensity threshold for image masks. To study the subtypes of adipocytes with unique phenotypes, the masks were then manually processed to select the target adipocytes. After the pixels of the cytoplasm were extracted by the image masks, the ORRs were calculated by dividing the total cytoplasmic signals recorded in the NADH channel by signals in the FAD channel. Because NADH and FAD fluorescence signals cannot be completely separated by the two detection channels (Figure S7), the

signal intensity in each channel did not strictly reflect the concentrations of each coenzyme. Since the minor crosstalk occurs mainly in the FAD channel, the changes in the ORR would be underestimated. Nevertheless, the ORR is still an effective biomarker to quantify the alterations of coenzyme concentrations, and can be used to characterize the NE-induced thermogenesis. SPCImage software (Becker and Hickl) was used to fit the FLT curves with a biexponential decay model ( $F(t) = a_1 e^{-t/\tau_1} + a_2 e^{-t/\tau_2}$ ) [42]. The free parameters include the short- ( $\tau_1$ ) and long- ( $\tau_2$ ) FLT components, and their relative contributions ( $a_1$  and  $a_2$ , where  $a_1 + a_2 = 100\%$ ). To generate FLIM images, the FLT in each pixel was calculated by biexponential fitting with pixel binning set as 3, and the total number of photons in the trace is around 2000. This pixel-wise fitting was used to visualize the FLT distributions in FLIM images. For more accurate assessment and statistics of the FLTs in each type of adipose tissues, all the cytoplasmic signals of the target adipocytes in each detection channel were extracted by corresponding image masks (Figure S6), and were summed to produce a single decay curve for biexponential fitting to obtain  $\tau_1$ ,  $\tau_2$ ,  $a_1$  and  $a_2$  [42]. This image-guided FLT analysis can achieve high signal-to-noise ratio fitting with more than 20 000 photons in the trace. To characterize the responses of NADH and FAD FLTs to NE, the time-resolved fluorescence images at the same site were captured before and at 30 min after NE injection, and then, the species fractions ratios ( $a_1/a_2$ ) in each image were analyzed. The error bars were calculated as the SEM values of all images obtained from four mice.

### 2.4 | Histology

Fat specimens were fixed in 0.5% paraformaldehyde (Electron Microscopy Sciences, RT15714) for 24 hours and processed following a standard paraffin embedding protocol. The paraffin-embedded adipose tissues were sectioned into 10  $\mu\text{m}$ , deparaffinized in 100% xylene and hydrated in 100% ethanol, 95% ethanol and 70% ethanol sequentially. For hematoxylin-eosin (H&E) staining, sections were stained with H&E followed by dehydration in 70% ethanol, 95% ethanol, 100% ethanol, 50% xylene with 50% ethanol and 100% xylene.

### 2.5 | Immunofluorescence staining

Fat specimens were sectioned into 6  $\mu\text{m}$ . The slides were blocked with 4% bovine serum albumin at PBS-T

(phosphate-buffered saline with 0.3% Triton) for 1 hour at room temperature and incubated with rabbit polyclonal UCP1 antibody (ab10983, Abcam, 1:200) at PBS-T overnight at 4°C. The slides were then washed with PBS-T and incubated with 1:1000 Alexa Fluor 594 donkey antirabbit antibody for 1 hour. DAPI (100 ng/mL 4',6-diamidino-2-phenylindole) was used as a counterstain. Immunofluorescence staining was observed using a Nikon upright fluorescence microscope.

## 2.6 | Western blotting

Dissected fat depots were homogenized in lysis buffer (50 mM Tris at pH 7.4, 10% glycerol, 1% Triton X-100, 150 mM NaCl, 1 mM EGTA, 1.5 mM MgCl<sub>2</sub>, 100 mM NaF, 20 mM PNPP, 20 mM β-glycerol phosphate, 50 μM sodium vanadate, 0.5 mM phenylmethylsulfonyl fluoride, 2 μg/mL aprotinin, 0.5 μg/mL leupeptin, 0.7 μg/mL pepstatin) by the homogenizer. The lysate was subjected to sodium dodecyl sulfate-polyacrylamide gel electrophoresis followed by transferring to a polyvinylidene difluoride membrane. The membrane was blocked with 10% nonfat milk in Tris-buffered saline with 1% Tween-20 for 1 hour and incubated with a primary antibody for 3 hours as well as in 5% nonfat milk containing a peroxidase conjugated secondary antibody (1:10000) for 1 hour. The primary antibodies and the dilution factors were listed below: anti-UCP1 (ab10983, Abcam, 1:10000) and anti-Tubulin (T4026, Sigma, 1:5000).

## 3 | RESULTS

### 3.1 | In vivo redox ratio imaging of beige fat

Our previous study showed that the thermogenesis in BAT could be detected based on the ORR measured with a spectroscope system [14]. However, this nonimaging approach cannot be directly used for metabolic monitoring of beige fat, because it cannot differentiate the beige adipocytes from the neighboring white adipocytes. In this study, we applied high-resolution multiphoton imaging to visualize the morphology of beige adipocytes in live mice and then accurately measured their ORRs using the image-guided metabolic analysis [31].

In the experiments, the mice were divided into two groups, as shown in Figure 1B. One group of mice was administered one dose of CL-316,243, an ADRB3 agonist to trigger the browning/beiging response in WAT, for seven consecutive days. In the other group, mice were treated with an equivalent volume of saline for the same

period. The H&E histology (Figure 1C) shows that beige adipocytes with multilocular structures were produced in the inguinal WAT depots after ADRB3 agonist administration for 1 week. Immunohistochemistry (Figure 1C) and western blotting (Figure 1D) also exhibit the generation of UCP1-abundant beige fat in the CL-316,243-treated mice. For in vivo TPEF imaging, the mouse skin around the inguinal region was removed to expose the adipose tissues. As shown in Figure 1A, the endogenous fluorescence signals of NADH and FAD in adipocytes were excited by an 810-nm femtosecond laser and were simultaneously collected by two separate detectors. The intensities of NADH and FAD fluorescence signals were used to calculate the ORR of the adipocytes. Meanwhile, the TCSPC module recorded the FLT and enables metabolic analysis in the time domain, which will be discussed in the following section. Figure 1E shows the representative pseudocolor TPEF images of inguinal fat of both CL-316,243 and saline-treated mice. The fluorescence signals in the NADH and FAD detection channels are coded in cyan and red, respectively. The LDs in the adipocytes can also be visualized by their intrinsic fluorescence, which exhibits a similar spectrum to NADH fluorescence [14]. The TPEF images show that the adipocytes in the saline-treated mice exhibit typical morphological features of WAT, which contain a single large LD surrounded by a thin layer of cytoplasm. On the other hand, multilocular beige adipocytes were observed in the inguinal fat of mice administrated with the ADRB3 agonist. The beige adipocytes are enriched with NADH and FAD fluorescence emitted from a large number of mitochondria in the cytoplasm, and the sizes of the LDs in the beige adipocytes are significantly smaller than those of the surrounding white adipocytes.

Next, we investigated the effect of thermogenesis on the redox ratio of beige adipocytes. Mice were injected with NE to activate thermogenic activity (Figure 1B). The time-lapse TPEF imaging recorded the changes of ORRs in the adipocytes over the whole course of NE-induced thermogenesis. Based on the TPEF images, the fluorescence signals in the cytoplasm of adipocytes were extracted for ORR analysis, while the lipid fluorescence was excluded using ratiometric image masks (Figure S6) [14]. It was found that the ORR of beige adipocytes increases by 14.5% in half an hour after NE injection (Figure 1F). The ORR rise during thermogenesis is associated with the biochemical transformation in the fatty acid β-oxidation, in which NADH is produced and FAD is consumed (Figure S1). It may also be correlated with the enhanced level of glycolysis, a metabolic pathway which is essential for thermogenesis in adipocytes and can elicit NADH production [43, 44]. Since ORR increase was also observed in BAT of mice after NE injection [14],

it indicates that the metabolic rate of brown and beige adipocytes during thermogenesis can be characterized by ORR measurement. In contrast, the ORR of white adipocytes remains stable over the same period. The results show that in vivo TPEF imaging provides a powerful means to resolve the morphological features of beige adipocytes embedded in WAT and to measure their metabolic dynamics during thermogenesis.

### 3.2 | In vivo FLIM imaging of adipose tissues

FLIM produces an image based on the exponential decay rate of fluorescence in the specimen, and it provides another angle to investigate cellular metabolism and its microenvironment. Taking advantage of the FLIM

system, we recorded time-resolved NADH and FAD fluorescence images of BAT, WAT and beige fat. It is well known that the free NADH signal exhibits a short FLT at 300 to 400 ps, while its FLT becomes much longer when binding to proteins [45]. In contrast, FAD signal possesses either a short or long FLT component depending on whether it is in a protein bound or free state, respectively [46]. The relative amplitudes of the free and protein-bound NADH and FAD have been found to be sensitive to the metabolic states of cells and tissues [33, 47]. Thus, we measured the free-to-bound ratios of NADH and FAD in adipose tissues in vivo and investigated their responses to thermogenesis.

The in vivo TPEF images of brown, beige and white fat are shown in the first column of Figure 2A. The corresponding NADH and FAD FLIM images are shown in the second and third column, respectively. To

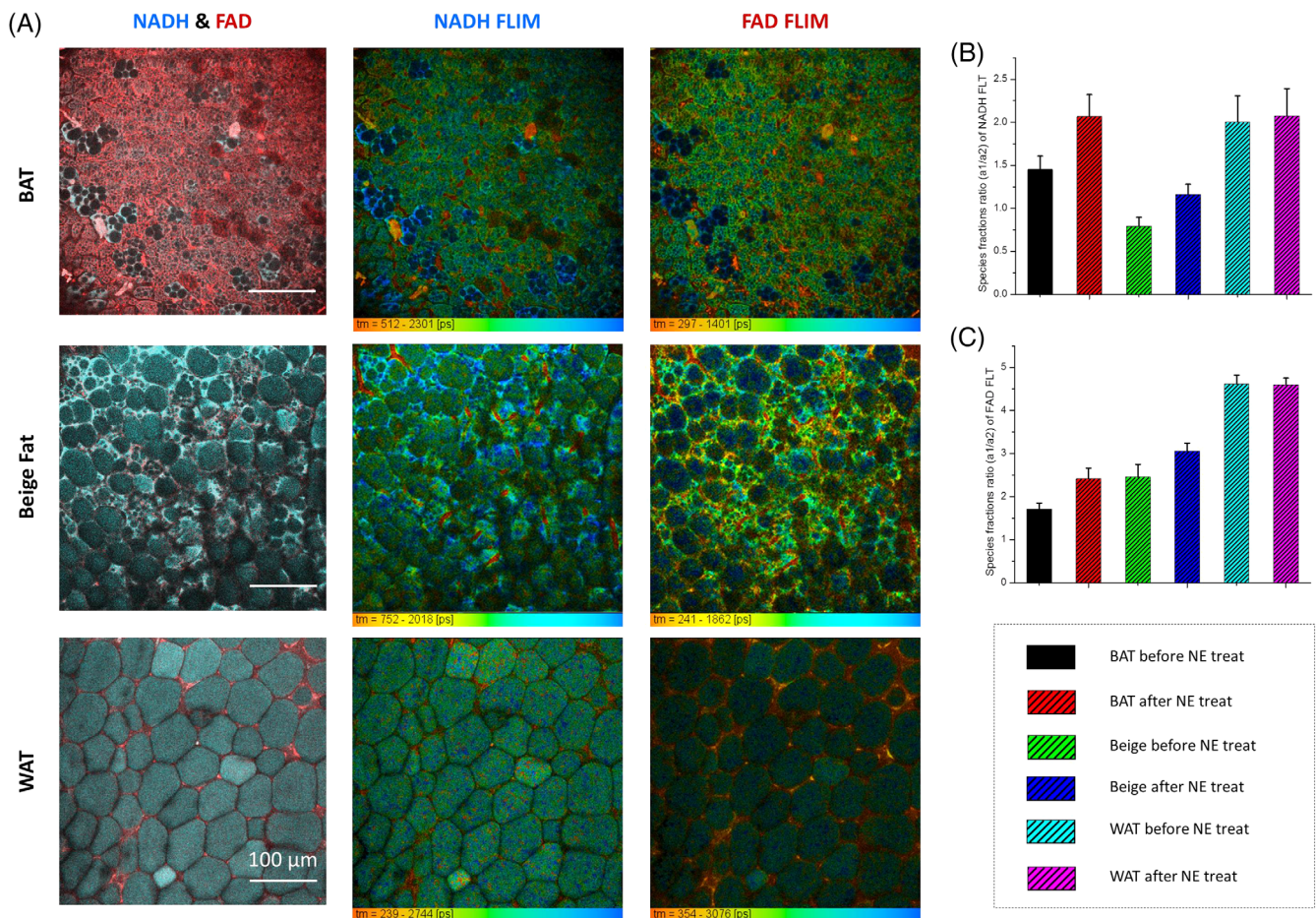


**FIGURE 2** In vivo FLT imaging of brown, beige and white fat. A, The FLT imaging of adipose tissues. First column, pseudocolor TPEF images of brown, beige and white fat, respectively; second column, NADH FLIM images of brown, beige and white fat, respectively; third column, FAD FLIM images of brown, beige and white fat, respectively. The color bars at the bottom of the FLIM images indicate the color coding of the FLT signals. B, The  $a_1/a_2$  values of NADH fluorescence of brown, beige and white fat before and after NE treatment.  $a_1$  and  $a_2$  are the amplitude coefficients of short- and long-FLT components in the biexponential decay fitting ( $F(t) = a_1 e^{-t/\tau_1} + a_2 e^{-t/\tau_2}$ ). C, The  $a_1/a_2$  values of FAD fluorescence of brown, beige and white fat before and after NE treatment. Each statistical bar in (B,C) is shown in terms of the average with the SEM over the measurements from four mice

accurately analyze the free-to-bound NADH and FAD in each type of fat, the fluorescence signals from all adipocytes in corresponding TPEF images were summed for biexponential fitting of FLT decay [42, 48]. Because beige adipocytes are heterogeneously distributed in the inguinal WAT depot, an image-guided FLT analysis was conducted to separate the newly generated thermogenic cells from the white adipocytes. The beige adipocytes were distinguished from white adipocytes based on their multilocular morphologies, and then their cytoplasmic autofluorescence signals were extracted for FLT fitting. The fluorescence of LDs in all adipocytes was excluded for FLT analysis using image masks (Figure S6). Figure 2B,C shows the ratios of short- and long-FLT components of NADH and FAD fluorescence in each type of adipocyte, respectively. Each mouse was injected with NE to activate thermogenesis, and the FLT at 30 min after NE injection was analyzed to compare with those before NE treatment. As shown in Figure 2B and Table S1, the  $a_1/a_2$  values of the NADH FLT in the brown and beige fat increase by 42.4% and 46.3%, respectively, after NE administration. It indicates that the relative contribution of the free NADH in these adipocytes rises significantly during thermogenesis. On the other hand, the free-to-bound NADH ratio in WAT remains stable after NE treatment. The rise in free NADH fraction in brown and beige fat may be attributed to the thermogenesis-elevated glycolysis which produces cytosolic NADH primarily in the free form (Figure S1) [36]. Meanwhile, the high  $\beta$ -oxidation levels and accumulated NADH in thermogenic adipocytes may promote a feedback pathway which transfers mitochondrial NADH to cytosol through the reversed malate-aspartate shuttle function to balance NADH/NAD<sup>+</sup> ratios [49]. Since the fluorescence quantum yield of NADH increase upon binding to proteins [50], the mitochondrial NADH generated in  $\beta$ -oxidation, which is mainly in protein-bound forms [36], has stronger fluorescence and would also contribute to the ORR increase in thermogenic adipocytes. As shown in Figure 2C and Table S2, the  $a_1/a_2$  values of the FAD FLT represent the bound-to-free FAD. It shows that the relative contribution of protein-bound FAD increases by 41.2% and 24.5% after NE treatment in brown and beige fat, respectively, while the FAD FLT components in WAT are not sensitive to NE. The increased contribution of bound FAD in thermogenic adipocytes may be due to the involvement of flavoproteins that bind to FAD, such as Acetyl-CoA-dehydrogenases, in the pathway of fatty acid  $\beta$ -oxidation [51]. Because protein-bound FAD usually has weaker fluorescence than the free forms [50, 52], the increased bound-to-free ratios of FAD would also lead to enhanced ORRs during thermogenesis. These results exhibit that NE-stimulated thermogenesis

enhances the relative contributions of free NADH and protein-bound FAD in the brown and beige fat, suggesting an association between thermogenesis and molecular changes in metabolic coenzymes in mitochondria. The results demonstrate that multiphoton FLIM is also capable for label-free characterization and detection of thermogenic activity in brown and beige fat in vivo. It provides additional information to redox ratio imaging in unraveling of metabolic dynamics in brown and beige fat.

### 3.3 | Heterogeneity in brown and beige fat

Beige and white adipocytes can undergo bidirectional interconversion under external stimulations [18, 53]. During the browning process, the unilocular white adipocytes with a single large LD will gradually transdifferentiate into multilocular phenotypes and acquire molecular characteristics of beige adipocytes. The in vivo multiphoton redox ratio and FLT imaging provided us the opportunity to investigate the diversity in morphology and metabolic capacity of beige adipocytes. As shown in Figure 3A, typical beige adipocytes with distinct structures of numerous small LDs can be observed in the inguinal fat of mice administrated with ADRB3 agonist. However, adipocytes with fewer and larger LDs are also present in the figure. The heterogeneity in morphology indicates that the cells could be at different transdifferentiation stages [18]. Interestingly, we found that brown adipocytes also exhibit heterogeneous morphology when performing in vivo TPEF imaging at interscapular BAT. As shown in Figure 3B, a group of cells display the classic appearance of brown adipocytes, which are enriched with cytoplasmic fluorescence emitted from densely packed mitochondria and contain large numbers of small LDs. In contrast, another group of brown adipocytes contain much larger LDs.

To study the metabolic heterogeneity in adipocytes, we classified the brown and beige adipocytes into four subgroups based on their morphologies, specifically the largest LD size in cell. Based on the analysis of LD size distribution, the thresholds of the largest LD size for cell classification were set as 10 and 25  $\mu\text{m}$  for the brown and beige adipocytes, respectively. The distributions of LD sizes in the four subgroups of adipocytes are shown in Figure 3C and Table S3, indicating that the thresholds could separate subgroups of cells sufficiently. We analyzed the ORR and FLT to assess the metabolic states of the adipocytes in each subgroup. It was found that brown adipocytes with larger LDs exhibit greater ORR values (Figure 3D and Table S3), which results from the dominant NADH fluorescence in the cytoplasm (Figure 3B).

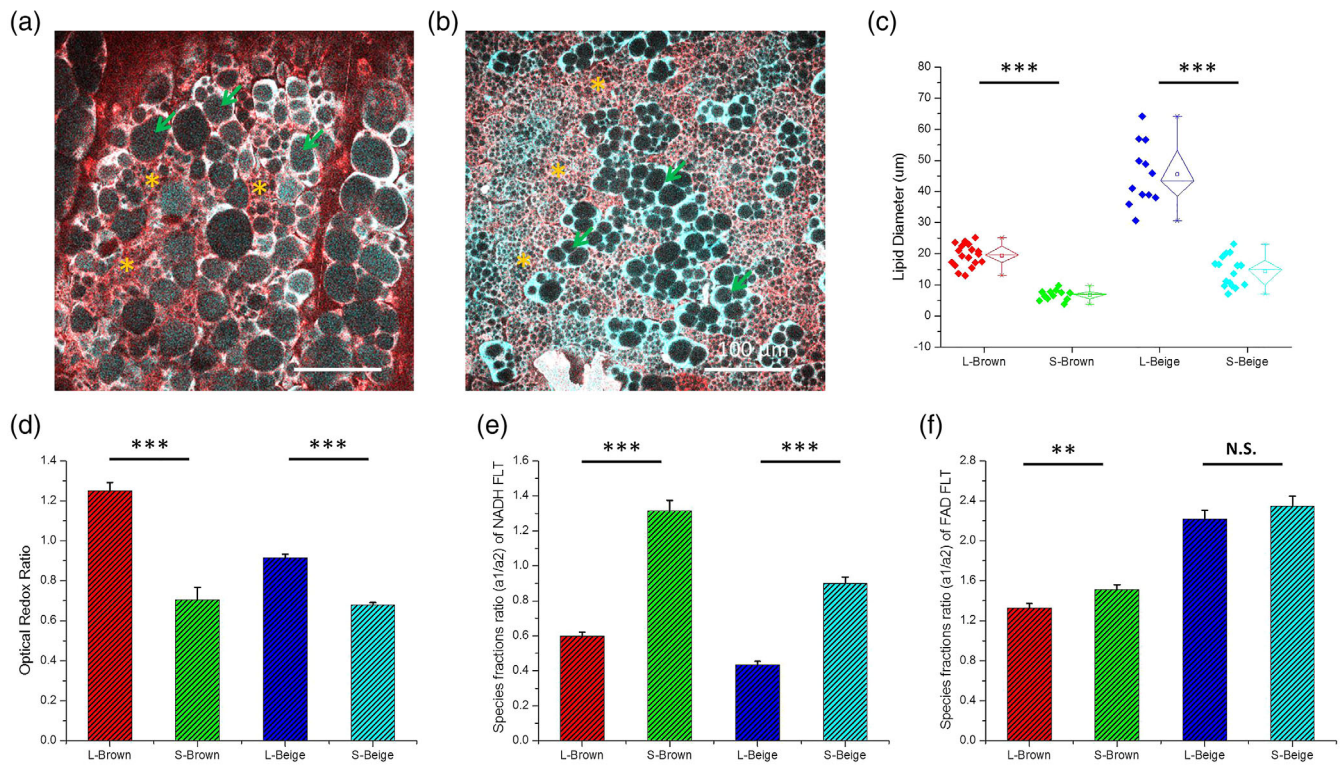


**FIGURE 3** In vivo TPEF imaging reveals heterogeneity in morphologies and metabolic states of brown and beige fat. A, The pseudocolor TPEF image of beige fat. The fluorescence signals in the NADH and FAD channels are coded in cyan and red, respectively. Adipocytes with distinct LD sizes are heterogeneously distributed in beige fat. Arrows: beige adipocytes with large LDs. Asterisks: beige adipocytes with small LDs. B, The pseudocolor TPEF image of brown fat. The fluorescence signals in the NADH and FAD channels are coded in cyan and red, respectively. Heterogeneity in LD size of adipocytes is also observed in BAT. Arrows: brown adipocytes with large LDs. Asterisks: brown adipocytes with small LDs. C, The statistics of LD diameters in each subgroup of brown and beige adipocytes. L-Brown: large-LD brown adipocytes; S-Brown: small-LD brown adipocytes; L-Beige: large-LD beige adipocytes; S-Beige: small-LD beige adipocytes. The subgroups of brown and beige adipocytes can be finely differentiated based on LD diameters. D, The ORRs of each subgroup of adipocyte. E, The  $a_1/a_2$  values of NADH FLT of each subgroup of adipocyte. F, The  $a_1/a_2$  values of FAD FLT of each subgroup of adipocyte. Each statistical bar in D-F is shown in terms of the average with the SEM over measurements from four mice. \*\*\* $P < .001$ ; \*\* $P < .01$

On the other hand, the brown adipocytes with numerous small LDs contain stronger FAD fluorescence and thus show lower ORR values. Similar to BAT, the ORRs of large-LD beige adipocytes are significantly higher than those of small LDs (Figure 3D).

Next, we analyzed the FLT of NADH and FAD fluorescence in each group of adipocyte. The results show that there is a significant difference in the free-to-bound NADH ratio between large-LD and small-LD adipocytes (Figure 3E and Table S3). The mean  $a_1/a_2$  values of the NADH FLT are 0.60 and 1.31 for large- and small-LD brown adipocytes, respectively. Similarly, the free-to-bound NADH ratio of the small-LD beige adipocytes is significantly higher than that of the large-LD cells. This indicates that the relative contributions of free NADH in small-LD brown and beige adipocytes are greater. As for the FAD fluorescence, the mean  $a_1/a_2$  values are 1.33 and 1.51 for large- and small-LD brown adipocytes,

respectively (Figure 3F and Table S3), suggesting a higher contribution of protein-bound FAD in small-LD brown adipocytes. In contrast, the relative amounts of free and bound FAD in the two groups of beige adipocytes show no significant difference. Our findings show significant heterogeneity in LD size distributions, ORRs and FLTs for thermogenic adipocytes in brown and beige fat.

The linear discriminant analysis exhibits that the subgroups of brown and beige adipocytes can be well distinguished based on their morphologies, ORRs and FLTs, as shown in Figure 4A-F. To investigate whether the diverse subgroups of adipocytes have distinct thermogenic capacities, we measured their metabolic responses to NE-stimulated thermogenesis using in vivo TPEF image-guided analysis. Specifically, large- and small-LD brown and beige adipocytes were identified in the TPEF images based on their morphologies. Then, the ORRs and FLTs of NADH and FAD were used as metabolic biomarkers to

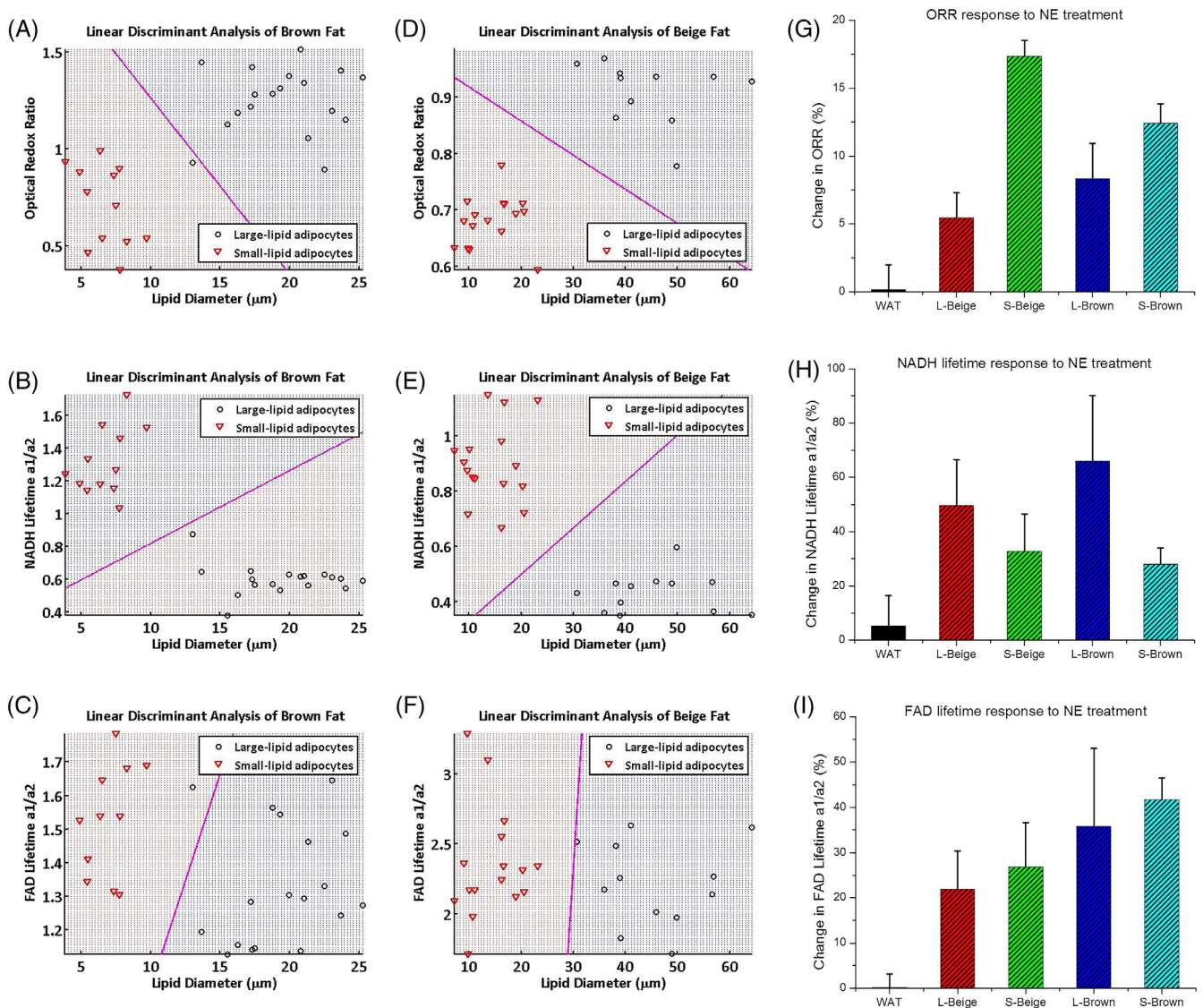


**FIGURE 4** Discrimination and metabolic characterization of brown and beige adipocytes. A, Scatterplot of lipid diameter and ORR for large- and small-LD brown adipocytes. B, Scatterplot of lipid diameter and NADH FLT for large- and small-LD brown adipocytes. C, Scatterplot of lipid diameter and FAD FLT for large- and small-LD brown adipocytes. D, Scatterplot of lipid diameter and ORR for large- and small-LD beige adipocytes. E, Scatterplot of lipid diameter and NADH FLT for large- and small-LD beige adipocytes. F, Scatterplot of lipid diameter and FAD FLT for large- and small-LD beige adipocytes. The discriminant lines in A-F distributed the two groups in two separate directions, indicating that the two subgroups of brown and beige adipocytes can be discriminated well based on the lipid diameters, ORRs and FLTs of NADH and FAD. G, ORR response to NE treatment in different types of adipocytes. H, NADH FLT ( $a_1/a_2$ ) response to NE treatment in different types of adipocytes. I, FAD FLT ( $a_1/a_2$ ) response to NE treatment in different types of adipocytes. Each statistical bar in G-I is shown in terms of the average with the SEM over the measurements from four mice

evaluate the NE-induced thermogenesis of adipocytes. As shown in Figure 4G and Table S4, the ORR of large-LD beige adipocytes increases by 5.5% after NE treatment, while the small-LD beige adipocytes exhibit a 17.4% rise in ORR over the same period. In BAT, the ORRs of small- and large-LD brown adipocytes rise by 12.4% and 8.3%, respectively, after NE treatment. These results suggest that the small-LD brown and beige adipocytes have higher thermogenic capacities than those with large LDs.

In addition to ORR, we measured the free-to-bound NADH and FAD ratios in each subgroup of adipocyte before and after NE treatment. It was uncovered that the increases in free-to-bound NADH ratio of large-LD beige and brown adipocytes are higher than those in small-LD ones (Figure 4H and Table S4). Meanwhile, although the relative contribution of protein-bound FAD increases in all four subgroups of adipocytes after NE injection, the difference in free-to-bound FAD ratio between the large-

and small-LD groups is not as significant as that in NADH fluorescence (Figure 4I and Table S4). It is also noticed that these metabolic biomarkers in white adipocytes have little response to thermogenesis, indicating that WAT is metabolically inactive.

## 4 | DISCUSSION

Although the metabolism of adipocytes has been extensively studied *ex vivo*, there is a lack of effective technologies enabling *in vivo* monitoring of the metabolic dynamics and heterogeneity in thermogenic adipocytes in live mouse model. Our recent work revealed a correlation between the browning level of WAT and its ORR response to NE-induced thermogenesis using a spectroscopy system [14]. However, the heterogeneously produced beige adipocytes make it impossible to precisely differentiate the redox states of the beige fat from the surrounding white fat. In this study, we used the label-free TPEF imaging for direct metabolic monitoring of beige adipocytes. To our knowledge, this is the first time that the thermogenesis of beige fat has been monitored *in vivo* at subcellular resolution. The fine morphological features of adipocytes resolved by TPEF imaging provide an indispensable guidance to identify the heterogeneously distributed beige adipocytes in inguinal fat and to precisely analyze their metabolic states. Compared to other techniques using exogenous fluorescent agents to measure the concentrations of coenzymes [54, 55], this label-free quantification approach can characterize the fluorescence intensity and FLT of molecules in a minimal invasive way, thus enabling accurate functional analysis in biological tissues.

The high-resolution TPEF imaging reveals subgroups of brown and beige adipocytes with distinct morphological and metabolic characteristics. It was found that the small-LD brown and beige adipocytes exhibit higher NE-induced ORR increases, suggesting their greater thermogenic capacities. On the other hand, the large-LD brown and beige adipocytes may have relatively lower ETC utilization, resulting in accumulation of NADH and higher base ORRs [56]. In addition, it is noticed that although the large-LD brown and beige adipocytes make less contribution to thermogenesis, they exhibit significant changes in NADH and FAD FLTs after NE treatment. This indicates that thermogenesis also regulates their intracellular metabolism and may induce considerable variations in the microenvironment of these cells, such as oxygen concentration, temperature and/or pH [47, 50, 57–59]. The possible reason for the heterogeneity in beige fat is that the large-LD beige adipocytes may correspond to those at early stages of transdifferentiation, which have similar properties to white adipocytes and thus show

weak thermogenic capacity. On the other hand, the small-LD beige adipocytes would be mature cells with strong thermogenic competence similar to brown adipocytes [18]. However, the mechanisms underlying the heterogeneity in BAT are still not clear. To completely unveil the reasons behind the correlations of LD size and thermogenesis, future studies combining the TPEF imaging and biomolecular analysis should be conducted to identify the gene signatures and molecular characteristics in each subgroup of adipocytes.

In sum, *in vivo* multiphoton redox ratio and FLT imaging produced structural and functional information to unravel the diverse metabolic characteristics of adipocytes. This technique provides a label-free and minimally invasive approach to evaluating the metabolic states and thermogenic capacities of adipose tissues *in vivo*. The subgroups of brown and beige adipocytes discovered by the high-resolution metabolic imaging could facilitate the understanding of heterogeneity in thermogenic competence and differentiation stages of adipocytes. By applying this metabolic monitoring technique to appropriate mouse models, novel therapeutic approaches to combat obesity and its related metabolic disorders by activating the thermogenic adipose tissues can be developed and assessed. Furthermore, it has been reported that adipose tissues also play crucial roles in inflammation and cancer [60], so the comprehensive study of the physiological and pathological characteristics of adipose tissues would completely decipher the contributions of adipocytes to systemic homeostasis and immune system.

## ACKNOWLEDGMENTS

This work was supported by the Hong Kong Research Grants Council through grants 662513, 16103215, 16148816, 16102518, T13-607/12R and T13-706/11-1, AOE/M-09/12, T13-605/18 W, C6002-17GF and Hong Kong University of Science and Technology (HKUST) through grant RPC10EG33.

## CONFLICT OF INTEREST

All the authors declare that they have no competing interests.

## ORCID

Sicong He  <https://orcid.org/0000-0002-0399-3904>

## REFERENCES

- [1] B. Cannon, J. Nedergaard, *Physiol. Rev.* **2004**, *84*(1), 277.
- [2] J. Ishibashi, P. Seale, *Science* **2010**, *328*(5982), 1113.
- [3] N. Petrovic, T. B. Walden, I. G. Shabalina, J. A. Timmons, B. Cannon, J. Nedergaard, *J. Biol. Chem.* **2010**, *285*(10), 7153.
- [4] J. Wu, P. Boström, L. M. Sparks, L. Ye, J. H. Choi, A.-H. Giang, M. Khandekar, K. A. Virtanen, P. Nuutila, G. Schaart, K. Huang, H. Tu, W. D. van Marken Lichtenbelt,

- J. Hoeks, S. Enerbäck, P. Schrauwen, B. M. Spiegelman, *Cell* **2012**, 150(2), 366.
- [5] P. Young, J. R. Arch, M. Ashwell, *FEBS Lett.* **1984**, 167(1), 10.
- [6] Y. Jiang, D. C. Berry, J. M. Graff, *Elife* **2017**, 6, e30329.
- [7] A. Fedorenko, P. V. Lishko, Y. Kirichok, *Cell* **2012**, 151(2), 400.
- [8] M. Harms, P. Seale, *Nat. Med.* **2013**, 19(10), 1252.
- [9] P. Cohen, B. M. Spiegelman, *Diabetes* **2015**, 64(7), 2346.
- [10] L. Sidossis, S. Kajimura, *J. Clin. Invest.* **2015**, 125(2), 478.
- [11] M. Trajkovski, K. Ahmed, C. C. Esau, M. Stoffel, *Nat. Cell Biol.* **2012**, 14(12), 1330.
- [12] X. Hui, P. Gu, J. Zhang, T. Nie, Y. Pan, D. Wu, T. Feng, C. Zhong, Y. Wang, K. S. L. Lam, A. Xu, *Cell Metab.* **2015**, 22(2), 279.
- [13] A. Matthias, K. B. Ohlson, J. M. Fredriksson, A. Jacobsson, J. Nedergaard, B. Cannon, *J. Biol. Chem.* **2000**, 275(33), 25073.
- [14] S. He, Y. An, X. Li, X. Wei, Q. Sun, Z. Wu, J. Y. Qu, *J. Biophotonics* **2018**, 11(8), e201800019.
- [15] T. F. Hany, E. Gharehpapagh, E. M. Kamel, A. Buck, J. Himms-Hagen, G. K. von Schulthess, *Eur. J. Nucl. Med. Mol. Imaging* **2002**, 29(10), 1393.
- [16] J. Reber, M. Willershäuser, A. Karlas, K. Paul-Yuan, G. Diot, D. Franz, T. Fromme, S. V. Ovsepian, N. Bézière, E. Dubikovskaya, D. C. Karampinos, C. Holzzapfel, H. Hauner, M. Klingenspor, V. Ntziachristos, *Cell Metab.* **2018**, 27(3), 689.
- [17] X. H. D. Chan, G. Balasundaram, A. B. E. Attia, J. L. Goggi, B. Ramasamy, W. Han, M. Olivo, S. Sugii, *J. Lipid Res.* **2018**, 59(6), 1071.
- [18] S. Altshuler-Keylin, K. Shinoda, Y. Hasegawa, K. Ikeda, H. Hong, Q. Kang, Y. Yang, R. M. Perera, J. Debnath, S. Kajimura, *Cell Metab.* **2016**, 24(3), 402.
- [19] T. Nagashima, H. Ohinata, A. Kuroshima, *Life Sci.* **1994**, 54(1), 17.
- [20] G. Abreu-Vieira, C. E. Hagberg, K. L. Spalding, B. Cannon, J. Nedergaard, *Am. J. Physiol. Endocrinol. Metab.* **2015**, 308(9), E822.
- [21] S. Keipert, M. Kutschke, M. Ost, T. Schwarzmayr, E. M. van Schothorst, D. Lamp, L. Brachthäuser, I. Hamp, S. E. Mazibuko, S. Hartwig, S. Lehr, E. Graf, O. Plettenburg, F. Neff, M. H. Tschöp, M. Jastroch, *Cell Metab.* **2017**, 26(2), 437.
- [22] S.-J. Lin, L. Guarente, *Curr. Opin. Cell Biol.* **2003**, 15(2), 241.
- [23] Q. Zhang, D. W. Piston, R. H. Goodman, *Science* **2002**, 295(5561), 1895.
- [24] A. A. Heikal, *Biomark. Med.* **2010**, 4(2), 241.
- [25] B. B. Lowell, B. M. Spiegelman, *Nature* **2000**, 404(6778), 652.
- [26] J. H. Ostrander, C. M. McMahon, S. Lem, S. R. Millon, J. Q. Brown, V. L. Seewaldt, N. Ramanujam, *Cancer Res.* **2010**, 70(11), 4759.
- [27] A. J. Walsh, R. S. Cook, M. E. Sanders, L. Aurisicchio, G. Ciliberto, C. L. Arteaga, M. C. Skala, *Cancer Res.* **2014**, 74(18), 5184.
- [28] M. Skala, N. Ramanujam, *Methods Mol. Biol.* **2010**, 594, 155.
- [29] W. Becker, *J. Microsc.* **2012**, 247(2), 119.
- [30] D. Chorvat, A. Chorvatova, *Eur. Biophys. J.* **2006**, 36(1), 73.
- [31] S. He, C. Ye, Q. Sun, C. K. S. Leung, J. Y. Qu, *Biomed. Opt. Express* **2015**, 6(3), 1055.
- [32] G. Yahav, S. Gershanov, M. Salmon-Divon, H. Ben-Zvi, G. Mircus, N. Goldenberg-Cohen, D. Fixler, *IEEE Trans. Biomed. Eng.* **2018**, 65(12), 2731.
- [33] M. C. Skala, K. M. Ricking, D. K. Bird, A. Gendron-Fitzpatrick, J. Eickhoff, K. W. Eliceiri, P. J. Keely, N. Ramanujam, *J. Biomed. Opt.* **2007**, 12(2), 024014.
- [34] D. K. Bird, L. Yan, K. M. Vrotsos, K. W. Eliceiri, E. M. Vaughan, P. J. Keely, J. G. White, N. Ramanujam, *Cancer Res.* **2005**, 65(19), 8766.
- [35] P. P. Provenzano, K. W. Eliceiri, P. J. Keely, *Clin. Exp. Metastasis* **2009**, 26(4), 357.
- [36] Z. Liu, D. Pouli, C. A. Alonzo, A. Varone, S. Karaliota, K. P. Quinn, K. Münger, K. P. Karalis, I. Georgakoudi, *Sci. Adv.* **2018**, 4(3), eaap9302.
- [37] C. A. Alonzo, S. Karaliota, D. Pouli, Z. Liu, K. P. Karalis, I. Georgakoudi, *Sci. Rep.* **2016**, 6, 31012.
- [38] Y. Wu, J. Y. Qu, *Opt. Lett.* **2005**, 30(22), 3045.
- [39] D. J. Bradley, M. H. R. Hutchinson, H. Koetser, T. Morrow, G. H. C. New, M. S. Petty, S. Tolansky, *Proc. R. Soc. London, A* **1972**, 328(1572), 97.
- [40] C. Xu, W. W. Webb, *J. Opt. Soc. Am. B* **1996**, 13(3), 481.
- [41] D. Fixler, Y. Namer, Y. Yishay, M. Deutsch, *I.E.E.E. Trans. Biomed. Eng.* **2006**, 53(6), 1141.
- [42] W. Becker, (fizik.) *The Bh TCSPC Handbook*, Becker & Hickl, Berlin, Germany, **2014**.
- [43] J. H. Jeong, J. S. Chang, Y.-H. Jo, *Sci. Rep.* **2018**, 8(1), 1.
- [44] A. Varone, J. Xylas, K. P. Quinn, D. Pouli, G. Sridharan, M. E. McLaughlin-Drubin, C. Alonzo, K. Lee, K. Münger, I. Georgakoudi, *Cancer Res.* **2014**, 74(11), 3067.
- [45] J. R. Lakowicz, H. Szmajcinski, K. Nowaczyk, M. L. Johnson, *Proc. Natl. Acad. Sci. U. S. A.* **1992**, 89(4), 1271.
- [46] S. Md, M. Islam, T. Honma, M. K. Nakabayashi, N. Ohta, *Int. J. Mol. Sci.* **2013**, 14(1), 1952.
- [47] M. C. Skala, K. M. Ricking, A. Gendron-Fitzpatrick, J. Eickhoff, K. W. Eliceiri, J. G. White, N. Ramanujam, *Proc. Natl. Acad. Sci. U. S. A.* **2007**, 104(49), 19494.
- [48] R. W. K. Leung, S.-C. A. Yeh, Q. Fang, *Biomed. Opt. Express* **2011**, 2(9), 2517.
- [49] L. Lumeng, J. Bremer, E. J. Davis, *J. Biol. Chem.* **1976**, 251(2), 277.
- [50] J. R. Lakowicz, *Principles of Fluorescence Spectroscopy*, 3rd ed., Springer, US **2006**.
- [51] S. O. Mansoorabadi, C. J. Thibodeaux, H. Liu, *J. Org. Chem.* **2007**, 72(17), 6329.
- [52] M. Y. Berezin, S. Achilefu, *Chem. Rev.* **2010**, 110(5), 2641.
- [53] M. Rosenwald, A. Perdikari, T. Rüllicke, C. Wolfrum, *Nat. Cell Biol.* **2013**, 15(6), 659.
- [54] O. Sallin, L. Reymond, C. Gondrand, F. Raith, B. Koch, K. Johnsson, *Elife* **2018**, 7, e32638.
- [55] O. Sallin, L. Reymond, and K. P. Johnsson, "Sensors, methods and kits for detecting nicotinamide adenine dinucleotides," World Intellectual Property Organization patent WO2016131833A1 (August 25, **2016**).
- [56] K. P. Quinn, G. V. Sridharan, R. S. Hayden, D. L. Kaplan, K. Lee, I. Georgakoudi, *Sci. Rep.* **2013**, 3, 3432.
- [57] B. Chance, B. Schoener, R. Oshino, F. Itshak, Y. Nakase, *J. Biol. Chem.* **1979**, 254(11), 4764.
- [58] K. Sato, Y. Nishina, K. Shiga, F. Tanaka, *J. Photochem. Photobiol. B* **2003**, 70(2), 67.
- [59] S. Ogikubo, T. Nakabayashi, T. Adachi, S. Md, T. Islam, M. K. Yoshizawa, N. Ohta, *J. Phys. Chem. B* **2011**, 115(34), 10385.

- [60] M. S. Desruisseaux, M. E. T. Nagajyothi, H. B. Tanowitz, P. E. Scherer, *Infect. Immun.* **2007**, 75(3), 1066.

### SUPPORTING INFORMATION

Additional supporting information may be found online in the Supporting Information section at the end of this article.

**How to cite this article:** He S, Wei X, Qin Z, Chen C, Wu Z, Qu JY. *In vivo* study of metabolic dynamics and heterogeneity in brown and beige fat by label-free multiphoton redox and fluorescence lifetime microscopy. *J. Biophotonics*. 2019; e201960057. <https://doi.org/10.1002/jbio.201960057>